

# ENTRY, DESCENT, AND LANDING GUIDANCE AND CONTROL APPROACHES TO SATISFY MARS HUMAN MISSION LANDING CRITERIA

Alicia Dwyer Cianciolo\* and Richard W. Powell†

Precision landing on Mars is a challenge. All Mars lander missions prior to the 2012 Mars Science Laboratory (MSL) had landing location uncertainty ellipses on the order of hundreds of kilometers. Sending humans to the surface of Mars will likely require multiple landers delivered in close proximity, which will in turn require orders of magnitude improvement in landing accuracy. MSL was the first Mars mission to use an Apollo-derived bank angle guidance to reduce the size of the landing ellipse. It utilized commanded bank angle magnitude to control total range and bank angle reversals to control cross range. A shortcoming of this bank angle guidance is that the open loop phase of flight created by use of bank reversals increases targeting errors. This paper presents a comparison of entry, descent and landing performance for a vehicle with a low lift-to-drag ratio using both bank angle control and an alternative guidance called Direct Force Control (DFC). DFC eliminates the open loop flight errors by directly controlling two forces independently, lift and side force. This permits independent control of down range and cross range. Performance results, evaluated using the Program to Optimize Simulated Trajectories (POST2), including propellant use and landing accuracy, are presented.

## INTRODUCTION

Precision landing on Mars is a guidance, navigation and control (GN&C) challenge. All Mars missions prior to the Mars Science Laboratory (MSL) flew unguided entry trajectories that resulted in landing location uncertainty ellipses on the order of hundreds of kilometers (see Figure 1). To land humans on the surface of Mars will require orders of magnitude improvement in landing accuracy over the MSL landing ellipse.

NASA's Evolvable Mars Campaign (EMC) has considered surface payload manifests to support a crew of four on the surface for 300 days.<sup>1</sup> Unlike the Design Reference Architecture 5.0 (DRA5) that assumed two 40 metric ton (t) payloads to multiple sites on Mars, the EMC considers four 20 t landers to a single site.<sup>2</sup> The EMC landers use a common descent stage and are required to deliver the payloads within a 50 m radius of a desired target site.

---

\* Aerospace Engineer, Atmospheric Flight and Entry Systems Branch (AFESB), NASA LaRC, Hampton VA 23681.

† Aerospace Engineer, AFESB, Analytical Mechanics and Associates MS 489 Hampton VA 23681.

The current Mars EDL state-of-the-art was demonstrated by MSL, which delivered a payload of nearly one ton (the Curiosity rover) to the surface of Mars with an accuracy of 12 x 4 mi (20 x 6 km). The vehicle entry mass was 3354 kg and jettisoned 150 kg of ballast mass to offset the center of gravity prior to entry such that the vehicle would fly with a lift-to-drag ratio (L/D) of 0.24 and a near-constant angle of attack of  $-14^\circ$ . During hypersonic flight, the vehicle used a reaction control system to modulate bank angle using thrusters, which controlled the orientation of the lift vector. The Apollo-derived guidance algorithm commanded a change in the lift vector that allowed the vehicle to minimize the cross range and down range to target a parachute deploy criteria of planet relative velocity of 580 m/s.<sup>3</sup> Just prior to parachute deploy, an additional 150 kg of mass was jettisoned to achieve the required angle of attack for parachute deployment. Once the parachute was deployed, the entry guidance was terminated. Subsonic retropropulsion continued to slow the entry and the sky crane lowered the rover to the surface. While the MSL preflight landing uncertainty ellipse was 20 x 6.5 km, the rover touched down within 3 km of the target in Gale Crater.<sup>4</sup>

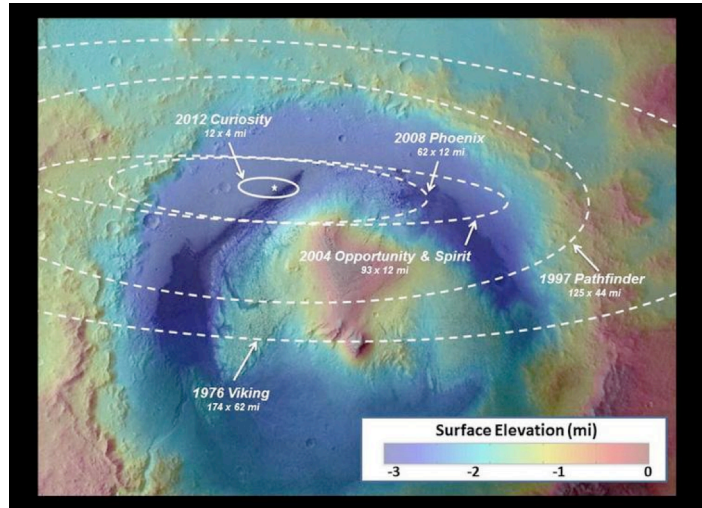


**Figure 1. Landing ellipse size relative to the lifted and guided entry of 2012 Curiosity mission.**

Despite the advancements demonstrated by MSL, many modifications to the current EDL state-of-the-art will be needed to accommodate human scale mission requirements at Mars. Due to the large entry masses (>40t) it is not practical for vehicles of this size to jettison ballast to adjust the center of gravity location needed to achieve the desired lift to drag ratio. Entry vehicles at this scale will not use parachutes for primary drag source during EDL. Instead, descent engines will be initiated at supersonic speeds to slow the vehicle for descent and landing replacing parachutes and the sky crane maneuver. Additionally, the months-long transit from Earth will mean that deceleration limits must be in place to protect the deconditioned crew. While robotic missions with parachutes can have peak entry decelerations exceeding ten Earth g's, the generalized maximum requirement assumed for Mars human scale EDL missions is four Earth g's. These limitations are based on couch position and duration at peak decelerations.<sup>5</sup> Furthermore, the large mass, the 50 m landing requirement, and the geometry of a supersonic retropropulsion trajectory necessitate modifications to sensors and landing strategies.

To meet the challenges of human scale missions several architectural and system design options exist. Three are presented the following sections: vehicle design, entry guidance strategies, and descent stage engine design. A discussion of how the relationships between these three aspects of EDL directly impact the mass and landing capability of the human scale system is also presented.

## HUMAN SCALE VEHICLE DESIGN

To achieve the desired lift and control required for human landing constraints, both low ( $<0.3$ ) and mid ( $\sim 0.5$ ) L/D vehicles have been considered. Work is ongoing to verify that mid L/D vehicles can achieve the EMC-defined landing constraint of 50 m to a target using bank angle control similar to Apollo and MSL. However, low L/D vehicles like MSL ( $L/D = 0.24$ ) will likely require more L/D as the mass, and therefore ballistic number, increases. Past studies have considered bank angle guidance for low L/D human scale vehicles.<sup>6</sup> To achieve adequate landing performance the vehicles have to fly with a higher L/D ( $\sim 0.3$ ) than the MSL vehicle. Therefore, the vehicle angle of attack must increase in magnitude from the  $-14^\circ$  of MSL to  $-22^\circ$ .

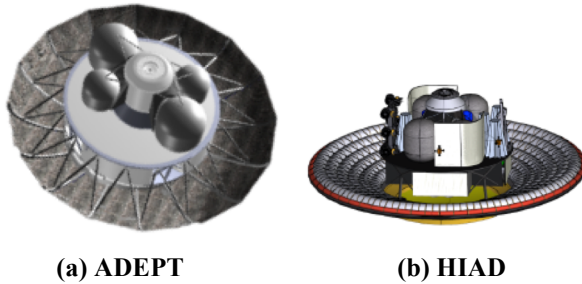


**Figure 2. Human scale low L/D vehicles.**

Entry and Placement Technology (ADEPT) and the second is an inflatable structure called Hypersonic Inflatable Aerodynamic Decelerator (HIAD).<sup>3,4</sup> Images of both vehicles are shown in Figure 2.

To reduce mass, no backshell covers the payload during aerocapture and EDL. The payload is protected by the large diameter heatshield. The lack of a backshell requires limiting the angle of attack range that the vehicle can fly due to concerns about flow impingement and radiative heating effects on the payload at high angles of attack. CFD was used to evaluate flow around generalize low L/D vehicle shapes with varying payload diameters and heights for various angles of attack. Two notional configurations at  $\alpha = 10^\circ$  and  $\alpha = 20^\circ$  are shown in Figure 3.

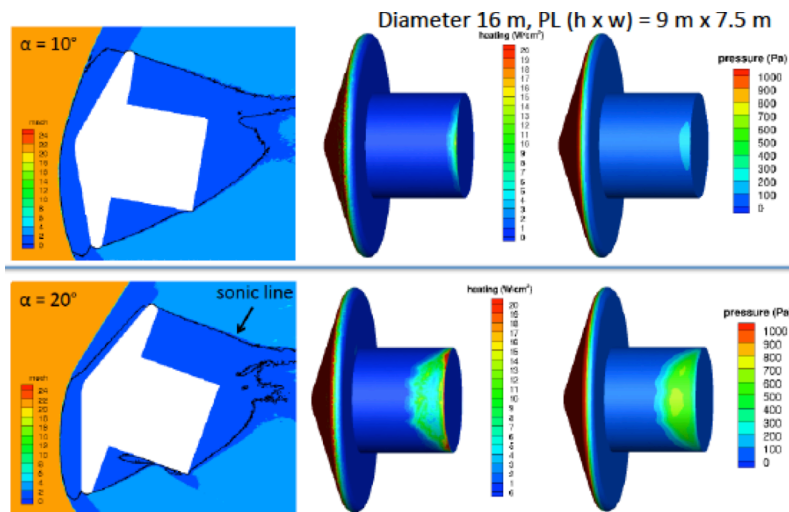


**Figure 3. Shock lines for notional Low L/D vehicle configurations.**

Note that the flow impingement at  $\alpha = 20^\circ$  impacts more of the payload (see bottom of the Figure 3) compared to the shallower  $\alpha = 10^\circ$  (in the top image of Figure 3). Other options to mitigate flow impingement include shortening the allowable payload height or increasing the de-

ployed diameter. While imposing a payload height limit may be a feasible approach, the actual payload configurations are not currently defined. Additionally, increasing the deployable diameter increases the mass of the system. Therefore, this paper will consider an approach that reduces the angle of attack while increasing the effective control authority to satisfy the EMC landing requirements. The following section will discuss two other system design options: entry guidance and descent stage engine design.

## **ENTRY GUIDANCE AND DESCENT STAGE ENGINE DESIGN**

Many design aspects of engines for Mars human scale missions are still being investigated. Aspects of the engines under consideration include propellant type, specific impulse, number of engines, orientation, thrust level per engine, cant angles, and gimbal or differential throttle capability. With this degree of design variability, system design considerations that simplify the engine requirements are advantageous.

Trajectory simulations have shown that the engines will likely have to be initiated between Mach 1.5 and 3. The thrust force of the engines dominates aerodynamic and atmosphere wind forces, making it tolerant to atmosphere dispersions. However, supersonic retropropulsion (SRP) uses a significant amount of propellant, which requires optimizing the initiation conditions to minimize propellant usage. Therefore, it is of interest to evaluate the potential entry guidance approaches that minimize the burden (propellant used and engine operational complexity) during the powered descent phase.

As mentioned previously, the EDL state-of-the-art includes bank angle guidance. Additionally, the open loop portion of flight that occurs during bank reversals decreases landing accuracy. Larger mass low L/D vehicles require higher L/D to achieve human scale performance requirements, and therefore have to fly at higher angles of attack, which increase the risk of flow impingement on the payload. Increasing the vehicle diameter to solve flow impingement concerns or relying on the descent stage engines to fly out both entry and navigation errors may substantially increase (on the order of metric tons) the mass of the entry system.

An alternative entry guidance, called Direct Force Control (DFC), is proposed and discussed in the following section. DFC addresses the bank angle guidance shortcomings while minimizing the burden on descent stage engines.

## **DIRECT FORCE CONTROL**

DFC as a method for EDL GN&C involves controlling individual forces directly during flight in independent directions. For this study, downrange is controlled with angle of attack modulation ( $\alpha$ ) and cross range is controlled by sideslip modulation ( $\beta$ ). The spacecraft coordinate frame showing  $\alpha$  and  $\beta$  is illustrated in Figure 4. In contrast, MSL used a modified Apollo entry guidance that adjusted bank angle magnitude for total range control and bank reversals to control cross range for most of the entry. Since angle of attack was not modulated, each bank reversal was an open-loop time segment.

Controlling forces in these two directions can be achieved in several ways. One way is to move the center of gravity by moving mass during flight. This was demonstrated on the IRVE III flight, in which the angle of attack was successfully modulated between  $0^\circ$  and  $2.5^\circ$ .<sup>9</sup> Another method that can change  $\alpha$  and  $\beta$  is to add aerodynamic flaps that can be modulated during flight, similar to a conventional airplane. Additional methods include modulating the forebody inflatable shape, inflating or deflating a flap, or using an asymmetric deployable device. Absent of a physical test article, this study simply assumes the performance of a notional flap mechanism (four

located 90° apart on the outer edge of the inflatable) and control system to achieve the desired DFC force modulation. The results compare the EDL performance, including landing accuracy and propellant used, to the heritage bank angle system on a similar vehicle. The following section describes the notional vehicle and concept of operations used for the comparison.

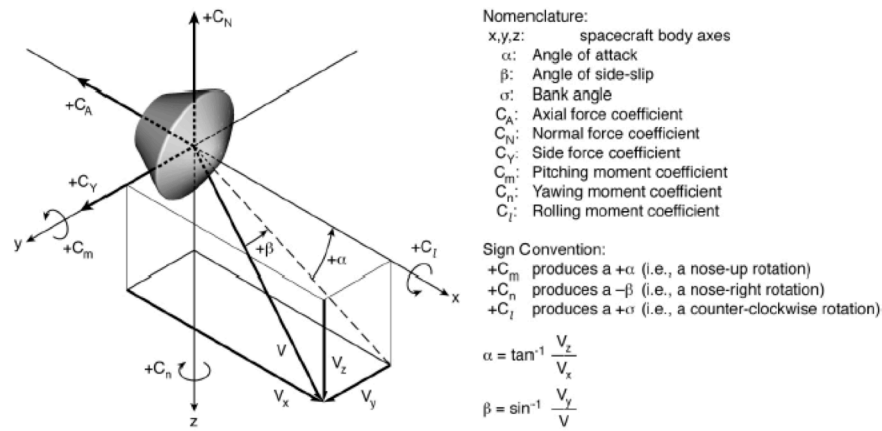


**Figure 4. Aerodynamic Coordinate Frame**

## EDL CONCEPT OF OPERATIONS

This study assumes that the Mars lander vehicle deorbits from the apoapsis of a highly elliptic 1 sol polar orbit (33,890 km x 250 km). A symmetric 70° sphere cone with a 16 m diameter represents the low L/D vehicle. The entry mass is assumed to be 51 t. The vehicle consists of a deployable attached to a descent module containing the engines, tanks, propellant, and landing legs. A 20 t Mars Ascent Vehicle (MAV) is attached to the descent stage module. The entry vehicle transitions to supersonic retropropulsion at a time selected by the simulation such that the vehicle can maintain a constant 2.5 m/s for five seconds prior to touching down at 0 km above the Mars Orbiter Laser Altimeter (MOLA) areoid. The descent stage has eight liquid oxygen and methane engines with 100 kN of thrust per engine and an Isp of 360 s. The landing site has not yet been selected, so this study assumes landing sites within 2° of the equator.

The vehicle utilizing bank angle control has an L/D = 0.32 and the center of gravity is located to achieve the required angle of attack of -20 degrees. No ballast jettison mass or vehicle asymmetry is modeled. The maximum bank rate is assumed to be 20°/s and the maximum bank acceleration is assumed to be 5°/s<sup>2</sup>.








The vehicle using DFC assumes that aerodynamic flaps can be modulated such that the maximum angle of attack rate is 5°/s and the maximum angle of attack acceleration is 2°/s<sup>2</sup>. Likewise, the maximum sideslip rate is 2°/s and the maximum sideslip acceleration is 0.3°/s<sup>2</sup>. This vehicle has an L/D = 0.22 such that the angle of attack remains less than 15 deg to minimize flow impingement on the payload.

The throttle of each of the eight 100 kN engines during the main propulsive phase may be commanded from 75% to 85% and the planet relative velocity angle of attack and sideslip could be commanded between ±0.1°. Once the constant velocity phase was reached the planet relative angle of attack and sideslip angles were set to 0° and the throttle setting modulated to maintain a velocity of 2.5 m/s. The following section describes the details of the entry guidance phases for both bank angle modulation and DFC approaches.

## Entry Guidance Overview

Both vehicles utilize a numerical predictor-corrector guidance algorithm based on one developed for the 2001 Mars Surveyor mission.<sup>10</sup> The algorithm is tuned for the nominal state and consists of four entry guidance phases, which are described below and summarized in Table 1. The vehicle mass properties are input to the simulation that runs the predictor-corrector algorithm. A description of the individual guidance phases is provided in this section.

**Table 1. Concept of Operations and Entry Guidance Phases**

	Entry Description	Phase	Bank Angle Guidance	Direct Force Control
	<b>Deorbit from apoapsis of 1 Sol Orbit</b> E - 11 hours <b>Entry Interface Occurs</b> Bank Angle E +0 s, Alt = 125 km, Inertial Vel = 4.7 km/s, inertial FPA = -10.4 deg DFC E +0 s, Alt = 125 km, Inertial Vel = 4.7 km/s, inertial FPA = -10.0 deg	#0 Deorbit	Entry Angle of Attack = -20° Entry Sideslip = 0 deg	Entry Angle of Attack = -14° Entry Sideslip = 0 deg
  	<b>Bank Angle: Acceleration Trigger 0.15 Earth g's</b> E + 91s, Mach =25, Alt =62 km, Range = 929 km <b>DFC: Acceleration Trigger 0.10 Earth g's</b> E + 88s, Mach = 25, Altitude = 66 km, Range = 813 km <b>Peak Heating Occurs</b> Bank Angle: E + 143s, Mach =20.7, Alt =36km, Range =694 km DFC: E + 146 s, Mach = 21, Alt = 39 km, Range = 548 km <b>Peak Load Occurs</b> Bank Angle: E + 164 s, Mach =17.4, Alt =31km, Range =610 km, g's = 2.9 DFC: E + 171s, Mach =17.1, Alt = 33km, Range = 451 km, g's = 2.8	#1 Accel Trigger	<b>Controls:</b> Bank angle magnitude and reversal time. <b>Targets:</b> Altitude, Velocity, heading and range at TAI	<b>Controls:</b> Angle of attack required to enter Terminal Area. <b>Targets:</b> Altitude, Velocity and range at TAI
	<b>Terminal Area Initiation</b> Bank Angle: E + 425 s, Mach =5.3, Alt =21 km, Range = 84 km DFC: E + 344 s, Mach = 5.3, Alt = 22 km, Range = 89 km	#2 Enter Terminal Area	<b>Controls:</b> Bank angle magnitude and reversal time, engine start time and vehicle angle of attack on engines <b>Targets:</b> Alt=12.5 m, Velocity= 2.5 m/s, constant throttle = 80% and down range =0 km	<b>Controls:</b> Angle of attack while engine are thrusting, engine start time <b>Targets:</b> Alt=12.5 m, Velocity= 2.5 m/s, constant throttle = 80% and down range =0 km
	<b>Engine Initiation</b> Bank Angle: E + 498s, Mach =2.9, Alt =7.4 km, Range =17.1 km DFC: E + 428 s, Mach = 2.7, Alt = 7.2 km, Range = 14.6 km	#3 Engine Start	<b>Controls:</b> engine throttle level, pitch and yaw angles <b>Targets:</b> Alt=12.5 m, Velocity= 2.5 m/s, down range = 0 km, cross range = 0 km	<b>Controls:</b> engine throttle level, pitch and yaw angles <b>Targets:</b> Alt=12.5 m, Velocity= 2.5 m/s, down range = 0 km, cross range = 0 km
	<b>Constant Velocity</b> Bank Angle: E + 553s, Alt =12.5 km, Vel = 2.5 m/s, Pitch = 0 deg, Yaw = 0 deg DFC: E + 481 s, Alt =12.5 km, Vel = 2.5 m/s, Pitch = 0 deg, yaw = 0 deg	#4 Constant Velocity Phase	Thrust modulated to maintain velocity = 2.5 m/s until touchdown at 0 km MOLA	Thrust modulated to maintain velocity = 2.5 m/s until touchdown at 0 km MOLA

Phase #0 – Deorbit: The vehicle trajectories for both the DFC and bank angle guidance case are initiated from apoapsis of a highly elliptic one-sol orbit with a deorbit burn. The vehicles are reoriented for entry to have the proper angle of attack prior to atmosphere entry. The simulation is allowed to select the size of the deorbit burn such that the landing constraints are satisfied. The size of the deorbit burn determines the entry flight path angle. No execution burn or navigation errors were included in the current analysis.

Phase #1 – Acceleration Trigger: Once in the atmosphere, the first guidance phase is triggered when the deceleration reaches 0.15 g's (bank angle control case) or 0.10 g's (DFC case). These values were chosen to ensure that the vehicle would be in continuum flow before activating the atmosphere and aerodynamics estimators used by the guidance algorithms. The bank angle control selects the magnitude of the bank angle and the time to perform the reversal to meet the altitude, velocity, heading and range constraints at the Terminal Area Initiation (TAI) point. The bank maneuvers are performed by a reaction control system. Likewise, DFC is allowed to command angle of attack and sideslip angle such that the same TAI constraints are met. Modification of angle of attack and sideslip are achieved by modulating flaps on the outer rim of the deployable vehicle.

Phase #2 – Enter Terminal Area: The terminal area is the target region sufficiently above the altitude required for engine initiation. During this phase the simulation controls engine start time and vehicle angle of attack (planet relative) during the thrust phase. A constant 80% engine thrust level is assumed for the guidance propagated trajectories. The targeted down range error at touchdown is zero kilometers.

Phase #3 – Engine Start: This guidance phase begins after engine initiation. The simulation controls the engine throttle level and the engine pitch and yaw angles (measured relative to planet-relative velocity vector) to fly out the entry errors. It is assumed that landing sensors will be able to determine the navigation errors and that the engines are capable of flying out those errors. Here the engine throttle level can vary between 75% and 85%. Using this throttle limit reduces engine performance requirements (deep throttling, gimbaling, etc.) and permits evaluation of the performance requirements of a system that uses aerodynamic forces rather than propellant to minimize targeting errors during entry.

Phase #4 – Constant Velocity Phase: Also called a “hover phase,” this occurs just before touchdown to ensure soft landing on safe terrain. Since landing sensors are not yet incorporated into the simulation, this phase provides conservatism to mitigate a divert or other maneuver to ensure safe landing. It is nominally designed to begin at 12.5 m above the surface and hold 2.5 m/s velocity for 5 s.

Only minor differences are noted in the reference profile for the bank angle and DFC cases. First, the reference profiles were designed with slightly different values for the Mars Global Reference Atmosphere Model (MarsGRAM) dust opacity parameter ( $\tau$ ). This resulted in slightly different entry flight path angles as shown in Table 1, in turn resulting in slightly different flight times. Priority was placed on developing robust guidance algorithms rather than ensuring identical entry parameters. Further tuning of both algorithms is needed as the system definition matures.

## Study Analysis

The simulation used for the evaluation was the Program to Optimize Simulated Trajectories II (POST2). POST2 was also used to evaluate the MSL EDL performance.<sup>4</sup> The study considers only 3 degrees of freedom and a fixed entry mass, so that any propellant used over the nominal trajectory reduces the payload delivery capability. Monte Carlo analysis is performed to compare

the two guidance and control approaches. Dispersions on the atmosphere, vehicle aerodynamics and mass are included in the simulation and are listed in Table 2.

As an additional stress parameter, a date that corresponded to a minimum in the atmospheric pressure cycle at Mars was selected for this analysis. This date was May 10, 2033, which corresponds to  $L_s = 164.1^\circ$ .

**Table 2. Monte Carlo Dispersions**

<b>Dispersion</b>	<b>Range</b>	<b>Distribution</b>
Atmosphere (MarsGRAM random number seed)	1:29999	Uniform
Atmosphere (MarsGRAM dust opacity parameter)	0.1-0.9	Uniform
Aerodynamics	MSL like	MSL like
Initial Mass	+/-50 kg	Uniform

## Results

This section presents the reference trajectories and summarizes the Monte Carlo results. Figures 5 through 10 show the reference trajectory parameters for both the bank angle control and DFC trajectories. Monte Carlo results include 8001 dispersed cases, with results shown in Figures 11 through 20.

Figure 5 shows the angle of attack for both reference trajectories. Notice that the bank angle guidance case, shown in green, holds a constant angle of attack near  $-20^\circ$  throughout the whole trajectory with the exception of the lowest velocities when the engines are activated. This constant angle of attack could result in flow impinging on the payload as previously described, and is one of the primary reasons for considering DFC. Notice in the same plot the DFC bank angle remains less than  $-10^\circ$  for nearly the entire trajectory. Note also the stairstep nature of the curve. This feature results from the fact that the guidance algorithm, using the rates and accelerations defined above, is updated in the simulation every 5 s. Further work using 6DOF analysis will refine the size of the flaps and determine if a physical mechanism can be controlled with the precision required in the simulation.

Sideslip angle is plotted in Figure 6. Note how the DFC reference simulation uses an immediate change in sideslip early in the trajectory (right side of the plot) to eliminate initial cross range error.

Figures 7 and 8 show reference bank angle and deceleration for the two trajectories. In Figure 7, the bank angle trajectory performs one reversal during the entry phase. It then performs a final reversal once it enters the terminal area (similar to a heading alignment phase). Figure 7 confirms that the DFC case does not use bank angle. To accommodate deconditioned crew, the reference trajectories are target peak entry  $g$ 's near 3 such that in the Monte Carlo analysis, no case will exceed 4  $g$ 's. The results are shown in Figure 8.

Figures 9 and 10 show altitude and lift to drag ratio versus velocity. In Figure 9, note that lofting in DFC case could be eliminated with further tuning and does not adversely impact the Monte Carlo results. The difference in L/D results from the vehicles flying at different angles of attack.



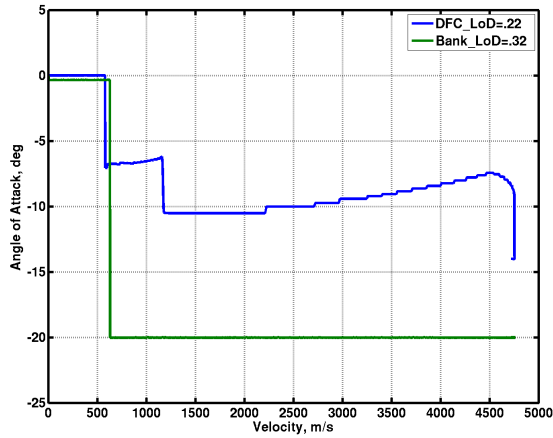


Figure 5. Reference Angle of attack vs. Velocity

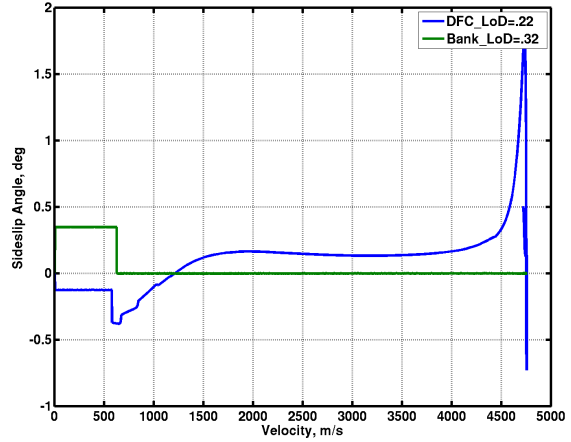


Figure 6. Reference Sideslip vs. Velocity

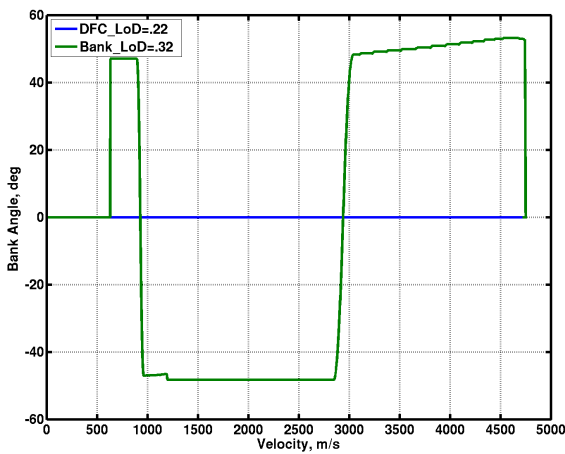


Figure 7. Bank angle vs. Velocity

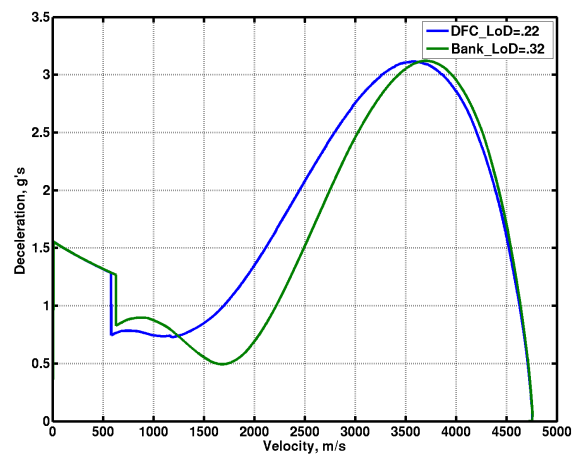


Figure 8. Deceleration vs. Velocity

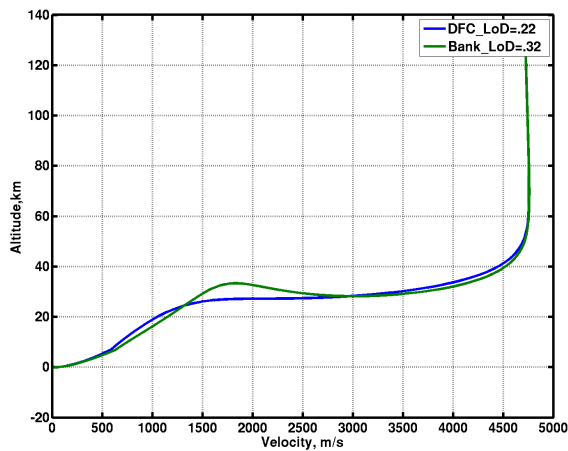


Figure 9. Reference altitude vs. velocity

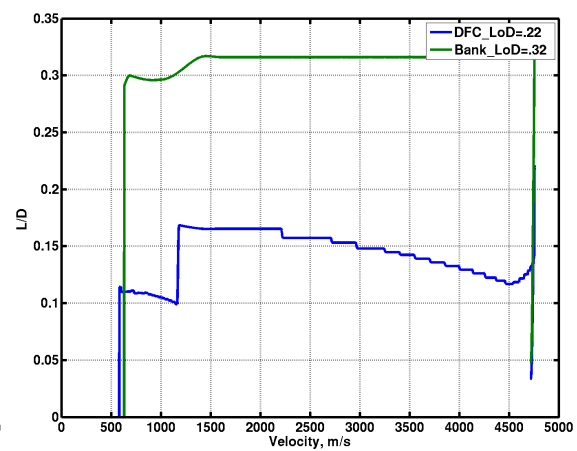


Figure 10. Lift-to-Drag ratio vs. velocity

Results for the Monte Carlo analysis are provided below. Figure 11 shows the final touch-down locations in latitude/longitude space for both guidance algorithms. Based on the assumptions made for this analysis, both entry guidance schemes meet the EMC requirement for landing

within 50 m of a target (denoted by the red dashed circle). The bank angle guidance had several cases with larger miss distances than DFC ( $>10$  m) but only one case did not meet the 50 m constraint. Figure 12 shows the histogram and statistics for the maximum total angle of attack during entry for both guidance approaches. As noted, lower angles of attack reduce the risk of flow impingement. DFC is able to meet the landing requirement while maintaining angle of attack less than  $15^\circ$ .

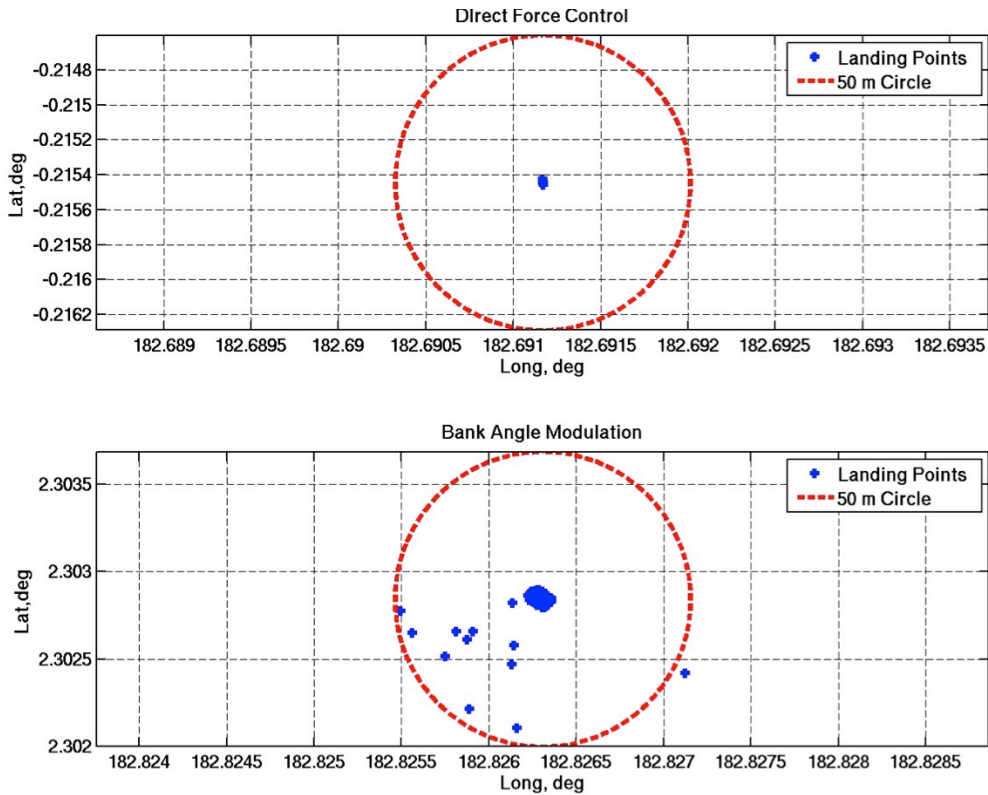


Figure 11. Landing footprints for both entry guidance algorithms.

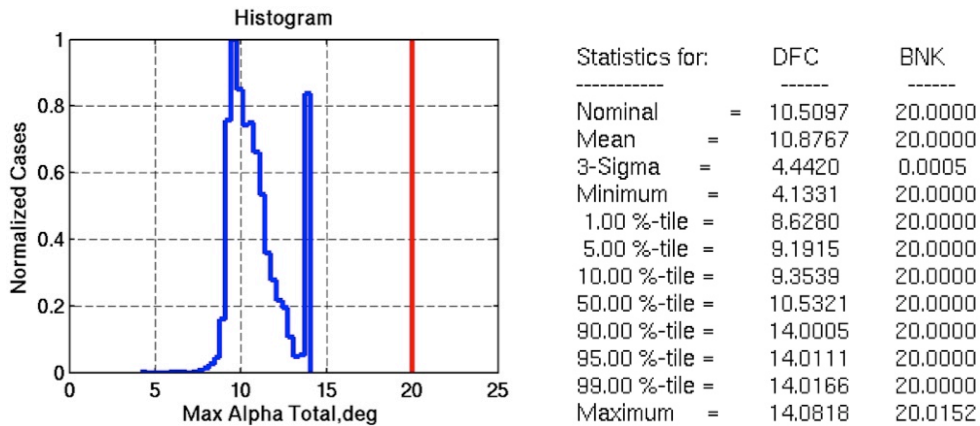


Figure 12. Landing footprints for both entry guidance algorithms.

Figure 13 shows the maximum L/D that occurs during flight. The variation in L/D in the DFC case results primarily from variations in angle of attack, though a small part is due to aerodynam-

ic dispersions. The variation in the L/D for the bank angle control case results primarily from the aerodynamic dispersion, since angle of attack is constant.

To meet the deceleration requirements for deconditioned crew, the reference trajectory for both guidance algorithms was designed to have a maximum deceleration of 3 Earth g's during entry. Therefore, when Monte Carlo dispersions are applied, the maximum does not exceed 4 Earth g's. Figure 14 shows the Monte Carlo results for maximum deceleration during entry.

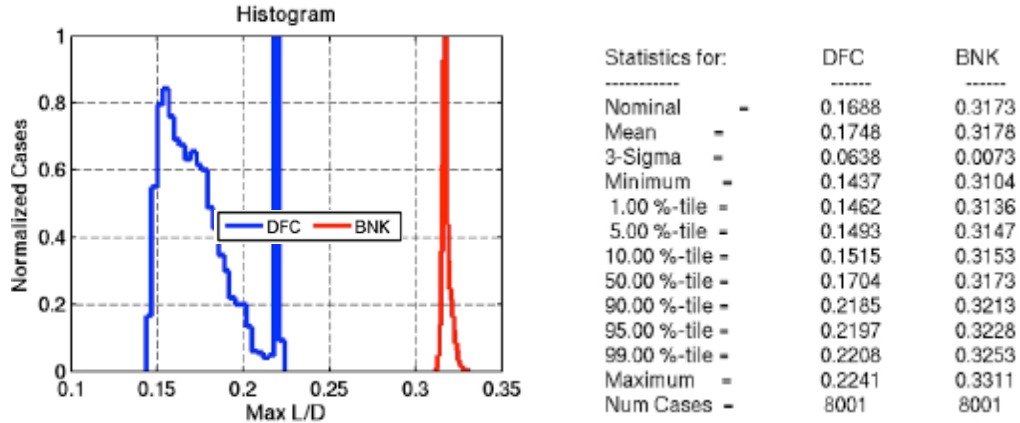


Figure 13. Maximum Lift to Drag ratio

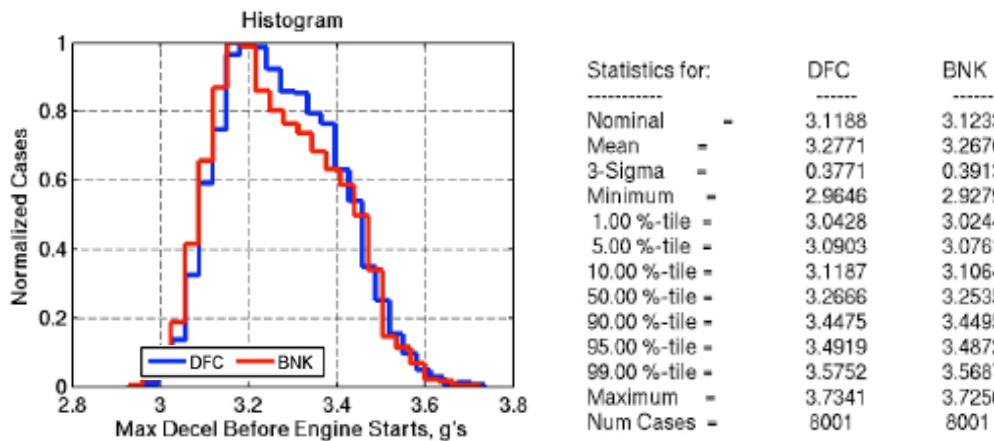


Figure 14. Maximum deceleration

Perhaps the most striking difference between the two guidance approaches is the propellant use shown in Figure 15. Note that a fixed entry mass was used in all cases so that the amount of propellant used over the nominal case would be considered a reduction in the payload capability of the system. If a system were designed to handle the 99% case, then the bank angle control case would need to have an additional 2 t of propellant to meet the same landing constraints as the DFC case, leading to a payload reduction of 2 t. Note also that the width of the distribution for propellant use is smaller for the DFC case, which is due to engine initiation start conditions. Figures 16 and 17 show the cloud of points in Mach and dynamic pressure space and Mach and altitude space, respectively. Notice how the bank angle cases have much broader distribution, primarily due to the fact that the vehicle flies open loop during the bank reversals. The atmosphere and aerodynamic dispersion are identical for both simulations. The plots also provide insight to the engine initiation environments. Again, the distribution is much smaller for DFC than for bank

angle in altitude, dynamic pressure and in Mach at engine initiation. Therefore the DFC cases spend less time on engines and use less propellant, as shown in Figure 18.

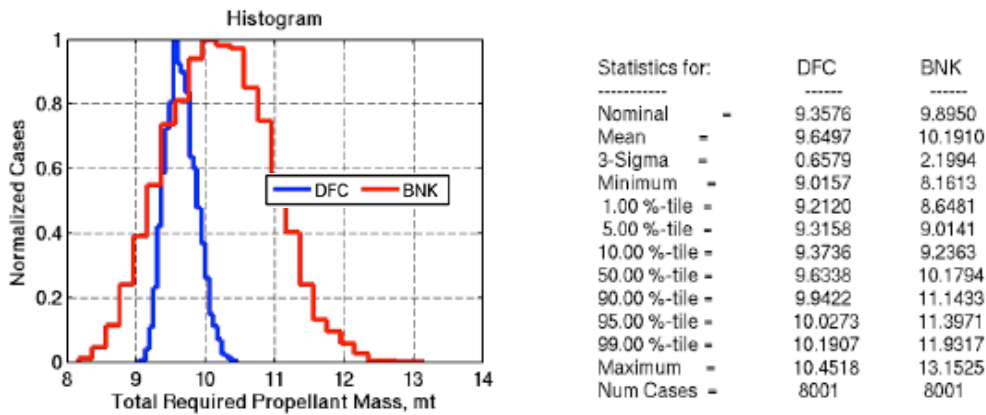


Figure 15. Propellant use.

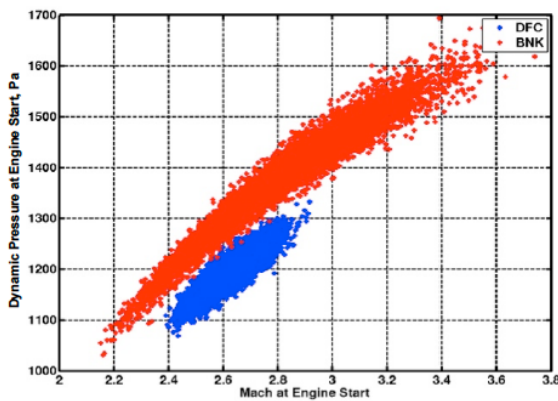


Figure 16. Dynamic Pressure vs. Mach

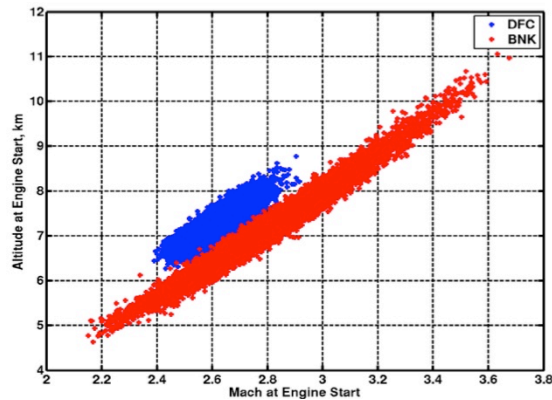
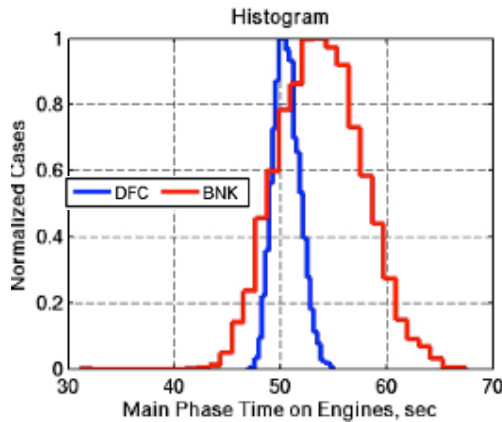


Figure 17. Altitude vs. Mach



Statistics for:	DFC	BNK
Nominal	48.9729	52.4771
Mean	50.6044	53.8273
3-Sigma	3.6737	11.5758
Minimum	46.9441	31.1369
1.00 %-tile	48.1449	45.8112
5.00 %-tile	48.7013	47.6925
10.00 %-tile	49.0628	48.8472
50.00 %-tile	50.5301	53.7279
90.00 %-tile	52.2454	58.8666
95.00 %-tile	52.7287	60.2908
99.00 %-tile	53.6100	63.1592
Maximum	55.0961	67.4411
Num Cases	8001	8001

Figure 18. Time on engines

In Phase 3 of the guidance scheme the descent engine throttle is allowed to vary from 75% to 80%. The vehicle selects the engine pitch and yaw angles required to meet the 50 m landing criteria. The purpose of monitoring these values was to determine engine performance requirements (e.g. cant angle, gimbal, thrust differential, depth of throttling) needed to meet the landing accuracy criteria. The Monte Carlo results and statistics shown in Figures 19 and 20 indicate that nei-

ther guidance algorithm required the engine angles to be greater than  $3^\circ$  (99%) at engine initiation. Thus, both algorithms deliver the vehicle to a point in space that permits a gravity turn terminal descent that is sufficient for landing, with no gimbal or differential throttling. The outliers shown in bottom plot in Figure 11 are the few cases that make up the tails of the bank angle (red) engine pitch and yaw angle histograms in Figure 19 and 20.

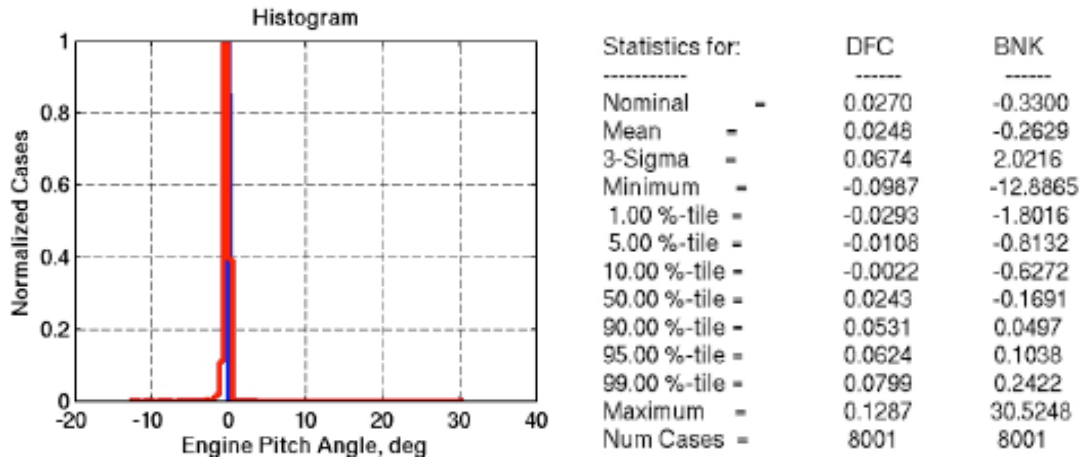


Figure 19. Engine pitch angle at initiation

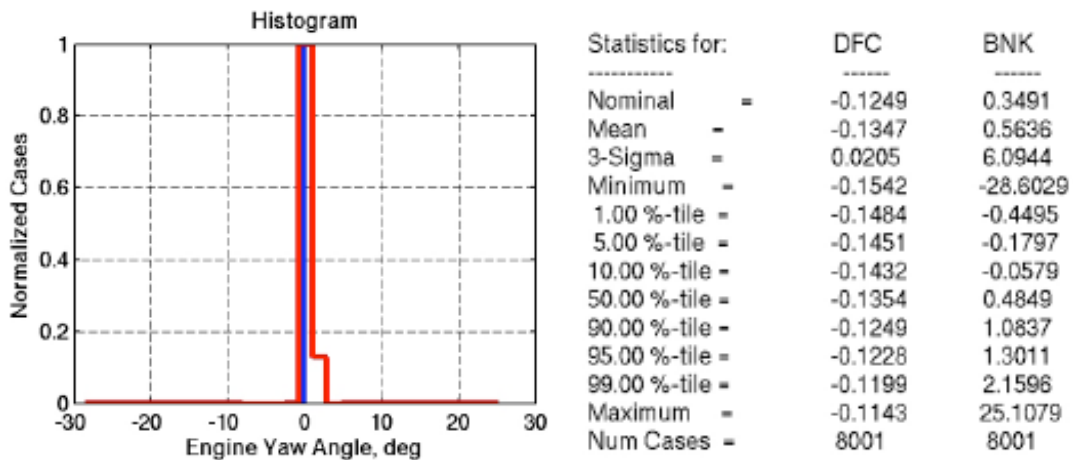


Figure 20. Engine yaw angle at initiation

## CONCLUSION

This paper reviewed the current state-of-the-art approach to landing on Mars. It also explained current assumptions being made for human scale Mars mission that change the EDL requirements, such as maintaining entry g's less than 4, delivering multiple vehicles in close proximity with 50 m accuracy, low L/D vehicles without a backshell, etc. The desire to minimize angle of attack during entry to reduce the risk of flow impingement on the payload has led to exploring new approaches to entry guidance, namely controlling forces in two directions (angle of attack and sideslip) rather than just one (bank angle). Many errors that affect the ability to perform precision landing can be eliminated during entry using the two-direction approach called Direct Force Control while also reducing performance requirements on the engines (e.g. requires no gimbaling, deep throttling, differential throttles, etc.).

Initial Monte Carlo results show that, while both bank angle control and DFC can achieve the 50 m landing requirement, bank angle control is more costly. DFC saves propellant, reduces landing dispersions, and reduces the burden on the engines. The analysis presented herein is based on the assumptions made for flap modulation rates and accelerations for a notional flap design. Results indicate that Direct Force Control offers benefits to human scale EDL that warrants further investigation and analysis. Future studies will investigate the effect of including additional dispersion (e.g. delivery errors, knowledge errors, deorbit burn execution errors, main engine start up transients, etc.) as well as engine out capability and 6DOF simulations that incorporate a controller to verify flap rates and accelerations. Once verified, mechanisms that meet the specifications will need to be identified. Eventually, a physical test of the system response will need to be performed if the DFC design continues to perform favorably in simulations.

## ACKNOWLEDGMENTS

The authors would like to acknowledge and thank Ashley Korzun of the NASA Langley Atmospheric Flight and Entry Systems Branch for running the CFD analysis to support the flow impingement analysis, part of which is presented in Figure 3.

## REFERENCES

- <sup>1</sup> L. Toups and S. Hoffman, "Pioneering Objectives and Activities on the Surface of Mars." AIAA-2015-4410. AIAA Space 2015 Conference. Pasadena, CA.
- <sup>2</sup> B. Drake. "Human Exploration of Mars: Design Reference Architecture 5.0." NASA/SP-2009-566A.
- <sup>3</sup> G.F. Mendeck and L. C. McGrew, "Post-Flight EDL Entry Guidance Performance of the 2011 Mars Science Laboratory Mission." AAS 13-419.
- <sup>4</sup> D.W. Way, J.L. Davis and J.D. Shidner, "Assessment of the Mars Science laboratory Entry, Descent and Landing Simulation." AAS 13-420.
- <sup>5</sup> "Constellation Program Human-System Integration Requirements." CxP 70024, 2006.
- <sup>6</sup> A.M. Dwyer Cianciolo, et al., "Entry, Descent and Landing Systems Analysis Study: Phase 1 Report," NASA-TM-2010-216720, July 2010.
- <sup>7</sup> A. Cassell, C. Brivkalns, J. Garcia, J. Bowles, D. Kinney, B. Yount, K. McGuire, P. Wercinski, A. Cianciolo, T. Polsgrove., "Human Mars Mission Design Study Utilizing the Adaptive Deployable Entry and Placement Technology," IEEE Aerospace Conference, Big Sky, MT 2017 (Abstract submitted)
- <sup>8</sup> S. Hughes, N. Cheatwood, A. Calomino, H. Wright, M. Wusk, M. Hughes, "Hypersonic Inflatable Aerodynamic Decelerator (HIAD) Technology Development Overview," 2013.
- <sup>9</sup> A.D. Olds, R. Beck, D. Bose, J. White, K. Edquist, B. Hollis, M. Lindell, and F.N. Cheatwood, "IRVE-3 Post Flight Reconstruction." AIAA-2013-3398.
- <sup>10</sup> R. W. Powell, "Numerical Roll Reversal Predictor Corrector Aerocapture and Precision Landing Guidance Algorithms for the Mars Surveyor Program 2001 Missions." AIAA 98-4574.